Available online at www.sciencedirect.com
ScienceDirect
Journal of Power Sources 175 (2008) 739–748
JOURNAL OF POWER SOURCES
www.elsevier.com/locate/jpowsour

$La_{0.4}Ce_{0.6}O_{1.8}$–$La_{0.8}Sr_{0.2}MnO_3$–8 mol% yttria-stabilized zirconia composite cathode for anode-supported solid oxide fuel cells

Min Zhang [a,b], Min Yang [a,b], Bin Liu [a,b], Zhifang Hou [a], Yonglai Dong [a], Mojie Cheng [a,*]

[a] *Dalian Institute of Chemical Physics, Chinese Academy of Sciences, 457 Zhongshan Road, Dalian 116023, PR China*
[b] *Graduate School of the Chinese Academy of Sciences, Beijing 100049, PR China*

Received 7 June 2007; received in revised form 30 September 2007; accepted 1 October 2007
Available online 12 October 2007

Abstract

The composite cathodes of $La_{0.4}Ce_{0.6}O_{1.8}$ (LDC)–$La_{0.8}Sr_{0.2}MnO_3$ (LSM)–8 mol% yttria-stabilized zirconia (YSZ) with different LDC contents were investigated for anode-supported solid oxide fuel cells with thin film YSZ electrolyte. The oxygen temperature-programmed desorption profiles of the LDC–LSM–YSZ composites indicate that the addition of LDC increases surface oxygen vacancies. The cell performance was improved largely after the addition of LDC, and the best cell performance was achieved on the cells with the composite cathodes containing 10 wt% or 15 wt% LDC. The electrode polarization resistance was reduced significantly after the addition of LDC. At 800 °C and 650 °C, the polarization resistances of the cell with a 10 wt% LDC composite cathode are 70% and 40% of those of the cell with a LSM–YSZ composite cathode, respectively. The impedance spectra show that the processes associated with the dissociative adsorption of oxygen and diffusion of oxygen intermediates and/or oxygen ions on LSM surface and transfer of oxygen species at triple phase boundaries are accelerated after the addition of LDC.

Keywords: Composite cathode; $La_{0.4}Ce_{0.6}O_{1.8}$; $La_{0.8}Sr_{0.2}MnO_3$; Solid oxide fuel cells

1. Introduction

Currently, intermediate temperature solid oxide fuel cells (IT-SOFCs, operated between 650 °C and 800 °C) have attracted intensive attention because the lowered operating temperature brings many benefits, such as increasing material selectivity and flexibility, improving stability and reliability of a SOFC system and lowering fabrication costs [1]. 8 mol% of yttria-stabilized zirconia (YSZ) is the most widely adopted electrolyte because of its high oxygen ion conductivity, good chemical stability, good mechanical stability and low fabrication cost, which is now fabricated into a thin electrolyte film for reducing ohmic resistance [2] and ensuring reliability for long-term applications [3].

$La_{1-x}Sr_xMnO_3$ (LSM) is an appropriate cathode material for a SOFC using YSZ electrolyte because of its good thermal and chemical compatibility with YSZ electrolyte and sufficient electrical conductivity [4]. Since the overpotential losses from O_2 reduction reaction on commonly used cathodes are relatively high in IT-SOFCs, the electrochemical activity of cathode material, which is related to the length of triple phase boundaries (TPBs), is a key issue to achieve high cell performance and maintain long-term stability [5,6]. To extend the electrochemical reaction zone from the two-dimensional interface between the electrolyte and the cathode to the three-dimensional bulk of the cathode, a composite cathode comprising LSM and YSZ is used to improve the cathode performance in practical applications [5,7,8]. Thus, the electrochemical reaction can occur within composite cathode at distances up to tens of micrometers from the cathode/electrolyte interface. LSM–YSZ composite cathode has good electrochemical activity for oxygen reduction at a temperature around 800 °C, but its electrochemical activity decreases seriously when temperature is below 700 °C. Therefore, the LSM–YSZ composite cathode cannot meet the requirements of IT-SOFCs.

Some alternative cathode materials with high ion conductivities and catalytic activities, such as $La_{1-x}Sr_xCoO_3$ [9], $La_{1-x}Sr_xCo_{1-y}Fe_yO_3$ [10], $Ba_{1-x}Sr_xCo_{1-y}Fe_yO_3$ [11,12] and

* Corresponding author. Tel.: +86 411 84379049; fax: +86 411 84379049.
E-mail address: mjcheng@dicp.ac.cn (M. Cheng).

0378-7753/$ – see front matter © 2007 Elsevier B.V. All rights reserved.
doi:10.1016/j.jpowsour.2007.10.012

$Sm_{1-x}Sr_xCoO_3$ [13], are applied to reduce the cathode polarization resistances (R_p) in IT-SOFCs. These materials react easily with YSZ during cell fabrication and/or operation processes to form insulated phases, and they are thermally mismatched with the YSZ electrolyte [14,15]. Thus, they cannot be directly applied onto the YSZ electrolyte. These problems can be solved by the following methods. One method is to prevent the reaction between these cathode materials and the YSZ electrolyte by adding a thin layer of doped ceria as a protective layer between the YSZ electrolyte and the cathode [16,17]. However, the added doped ceria layer may react with YSZ electrolyte to form an insulated solid solution, which results in an increase of ohmic resistance (R_{ohm}) [18]. Furthermore, an additional layer increases the complexity of cell structure and fabrication cost. Another method is to improve the electrochemical activity for oxygen reduction of LSM cathode by introducing some active components into LSM cathode, such as the impregnation of $La_{0.5}Sr_{0.5}CoO_3$, $LaCoO_3$ or $LaNi_{0.6}Fe_{0.4}O_3$ into the LSM cathode [19] and the infiltration of cobalt into LSM–$(Sc_2O_3)_{0.1}(Y_2O_3)_{0.01}(ZrO_2)_{0.89}$ composite cathode [20].

Since the low electrochemical activity of LSM–YSZ composite cathode in low temperature range arises from the low ion conductivity and low oxygen reduction activity, it can also be improved through the electrolyte choice in the composite cathode. In our previous work, we reported that using ScSZ as an ion conductor other than YSZ in the composite cathode reduced the R_p, especially in the low temperature range [21]. It was indicated that the ceria doped in the ScSZ electrolyte also contributed to the oxygen reduction processes. Here we demonstrate a new strategy to obtain high cell performance for IT-SOFCs through introducing $La_{0.4}Ce_{0.6}O_{1.8}$ (LDC) into LSM–YSZ composite cathode and investigate the reason for the increased electrochemical activities.

2. Experimental

2.1. Powder synthesis

$La_{0.8}Sr_{0.2}MnO_3$ (LSM) was synthesized by an EDTA–citric acid method with La_2O_3 (99.99%), $Sr(NO_3)_2$ (99.5%), $Mn(NO_3)_2$ solution (49–51%) as raw materials, and calcined at 1100 °C for 3 h to form pure perovskite phase and suitable particle size distribution. $La_{0.4}Ce_{0.6}O_{1.8}$ (LDC) was synthesized by the same method as LSM with La_2O_3 (99.99%), CeO_2 (99.9%) as raw materials, and calcined at 700 °C for 2 h to form pure cubic fluorite structure.

2.2. Cell fabrication

YSZ (from Tosoh) and NiO (from J.T. Baker) were used to prepare Ni/YSZ anode substrates. YSZ and NiO in a weight ratio of 50:50 were mixed through grinding in a mortar. Then, suitable organic binders and *n*-butanol solvent were added and the mixture was fabricated into anode substrate via a tape-casting process. YSZ powder was mixed with organic binder and plasticizer to form YSZ colloidal suspension. YSZ colloidal suspension was applied onto one side of the anode substrate by a slurry coating method. The anode/electrolyte assembly obtained were drilled into discs. The discs were then sintered at 1400 °C for 2 h in air. The sintered discs were ca. 21 mm in diameter and 450 μm in thickness. The thickness of the YSZ electrolyte film was ca. 15 μm.

LSM and YSZ in a weight ratio of 60:40 were used to prepare the composites. LDC was added to the composites with a content ranging from 1 wt% to 50 wt% of the total mass of LSM and YSZ. The mixtures of LDC, LSM and YSZ were ground thoroughly in ethanol to form an ink-like mixture. A series of composites with different LDC contents were obtained after drying, denoted as *x* wt% LDC–LSM–YSZ where *x* represents the content of LDC. The cathode pastes were prepared from mixing of these composites with organic binders and *n*-butanol solvent. The cathodes were screen-printed onto the YSZ films using the pastes, and fired at 1200 °C for 2 h in air. The cathode had an effective area of about 0.6 cm^2 and a thickness of about 20 μm.

2.3. Oxygen temperature-programmed desorption (O_2-TPD)

The O_2-TPD experiments were carried out in a system equipped with a Balzers Omnistar™ mass spectrometer. To simulate the interaction of different materials in the composite cathodes, the samples of LSM, LDC, LSM–YSZ and *x* wt% LDC–LSM–YSZ were fired at 1200 °C for 2 h. Each sample (200 mg, loaded in a quartz tubular micro-reactor) was pretreated in pure O_2 with a flow rate of 50 ml min^{-1} at 800 °C for 1 h. The sample was cooled down to room temperature in the same atmosphere and then purged with high pure He gas (≥99.999 vol.%, 50 ml min^{-1}) until the baseline became level. Then, O_2-TPD measurement was performed from 30 °C to 960 °C with a heating rate of 10 °C min^{-1} and a He flow of 50 ml min^{-1}. The sample was held at the maximal temperature for 30 min.

2.4. Cell testing and microstructure characterization

The single cells were tested on a home-made test station. The cell was placed between two quartz tubes. Silver meshes were adopted as current collectors, and silver wires welded on silver meshes were used both as current and voltage probes. Hydrogen, bubbled through water at room temperature, was supplied to the anode as fuel gas, and pure O_2 was supplied to the cathode as oxidant gas. Both gases were kept at the same flow rate of 100 ml min^{-1} by mass flow controllers. The electrochemical impedance spectra (EIS) measurements were carried out under open circuit conditions on a Solartron 1287 potentiostat and a 1260 frequency response analyzer. The frequency ranged from 100 kHz to 0.015 Hz with a signal amplitude of 10 mV.

The microstructures of the composite cathodes after cell test were examined by a Quanta 200 FEG (FEI Company) scanning electron microscope equipped with energy dispersive X-ray (EDX) spectroscopy.

3. Results and discussion

3.1. O_2-TPD behaviors

O_2-TPD is an effective method to investigate the behaviors of oxygen species in a perovskite-type oxide through monitoring gas phase oxygen desorbed from a pre-treated oxide sample with temperature increases. Commonly for ABO_3 perovskite-type oxides, there are two kinds of desorption peaks in their O_2-TPD profiles. The peaks in lower temperature range are attributed to the desorption of α (α′)-oxygen which is oxygen ordinarily chemically adsorbed on the surface or surface oxygen vacancies. The peaks in higher temperature range are ascribed to the desorption of β (β′)-oxygen which is the bulk oxygen [22]. The desorption behavior of β (β′)-oxygen depends on the nature of the B cation, being correlated to its partial reduction to lower oxidation states, and it is generally considered as a criteria of bulk oxygen mobility in the material.

Fig. 1 gives the O_2-TPD profiles of the LSM, LDC, LSM–YSZ and LDC–LSM–YSZ samples with different LDC contents. For the LSM sample, only one desorption peak centering at 815 °C is observed, which corresponds to oxygen (β-oxygen) escaped from the lattice with the reduction of Mn^{4+} to Mn^{3+}. LSM material is quite different from the other 3d metal-containing perovskites on which two O_2-TPD peaks for the Ni- and Fe-containing perovskites [23] and three O_2-TPD peaks for the Co-containing perovskites are observed [24]. Because $La_{0.8}Sr_{0.2}MnO_3$ displays an oxygen-excess at $P(O_2)$ be higher than 10^{-5} atm when temperature is below 1000 °C [25,26], there is no α′-oxygen desorption peak in its O_2-TPD profile. For the LDC sample, no oxygen desorption peak is observed in its O_2-TPD profile, which is similar with the O_2-TPD result of $Ce_{0.8}Y_{0.2}O_{1.9}$ material reported by Luo et al. [27].

On the LSM–YSZ sample, a desorption peak located at low temperature (ca. 395 °C) is observed, which can be ascribed to the desorption of ordinarily chemically adsorbed oxygen ($O_2^{\delta-}$, α-oxygen) on the surfaces. The amount of oxygen desorbed at this temperature is correlated to the specific surface area of a sample [23]. The very weak shoulder at 420–620 °C is ascribed to the liberation of oxygen (α′-oxygen) adsorbed on the oxygen vacancies which are created on LSM surfaces due to the introducing of YSZ as Eqs. (1) and (2) show

$$O^x_{O,LSM} + 2Mn^{\bullet}_{Mn,LSM} + V^{\bullet\bullet}_{O,YSZ} + 2e' \rightarrow V^{\bullet\bullet}_{O,LSM} + 2Mn^x_{Mn,LSM} + O^x_{O,YSZ} \quad (1)$$

$$O^x_{O,LSM} + 2Mn^x_{Mn,LSM} + V^{\bullet\bullet}_{O,YSZ} + 2e' \rightarrow V^{\bullet\bullet}_{O,LSM} + 2Mn'_{Mn,LSM} + O^x_{O,YSZ} \quad (2)$$

where $O^x_{O,LSM}$ and $O^x_{O,YSZ}$ represent the O^{2-} ions in LSM and YSZ lattice sites; $V^{\bullet\bullet}_{O,LSM}$ and $V^{\bullet\bullet}_{O,YSZ}$ stand for oxygen vacancies; $Mn^{\bullet}_{Mn,LSM}$, $Mn^x_{Mn,LSM}$ and $Mn'_{Mn,LSM}$ are Mn^{4+}, Mn^{3+} and Mn^{2+} ions, respectively.

At the same time, oxygen vacancies created on the LSM surfaces promote oxygen migration from bulk to surface, which is confirmed by the following facts. First, the LSM–YSZ sample gives a higher amount of β-oxygen than the LSM sample, which is depicted by the larger area of the main peak at 815 °C in the O_2-TPD profile of LSM–YSZ sample. The calculation result shows that the amount of β-oxygen desorbed from unit weight LSM in the LSM–YSZ sample is about 1.5 times of that in the LSM sample. Secondly, a weak shoulder at ca. 960 °C appears on the LSM–YSZ sample, which was also observed by other researchers [28]. It was suggested that Mn^{4+} in $La_{1-x}Sr_xMnO_3$ could be reduced to Mn^{3+} and further to Mn^{2+} at very low oxygen partial pressures [26]. Therefore, the shoulder at ca. 960 °C can be reasonably attributed to the desorption of oxygen (β′-oxygen) accompanying with the reduction of some Mn^{3+} to Mn^{2+} due to the accelerated mobility of bulk oxygen. The very weak peak at ca. 960 °C and the well-retained perovskite structure of the samples after O_2-TPD experiments indicates that only quite a small portion of Mn^{3+} was reduced.

In the O_2-TPD profiles of the LDC–LSM–YSZ samples, the oxygen desorption peaks appear at the same temperatures as the LSM–YSZ sample, and it is reasonable to give the same attribution of these peaks as the LSM–YSZ sample. It can be observed that the weak shoulder peak at 420–620 °C becomes stronger with the increase of LDC content, which indicates more surface oxygen vacancies are created on the samples. It could be concluded rationally that the special redox property of LDC, i.e. the easy interconversion of Ce^{4+} and Ce^{3+}, makes more oxygen vacancies be created on LSM surfaces. Accordingly, in their O_2-TPD profiles the main peak at 815 °C also becomes larger and wider. The area of the peak at 815 °C on the 5 wt% LDC–LSM–YSZ sample is about two times of that on LSM sample calculated based on unit weight LSM, indicating that oxygen vacancies created on LSM surfaces accelerate the mobility of bulk oxygen.

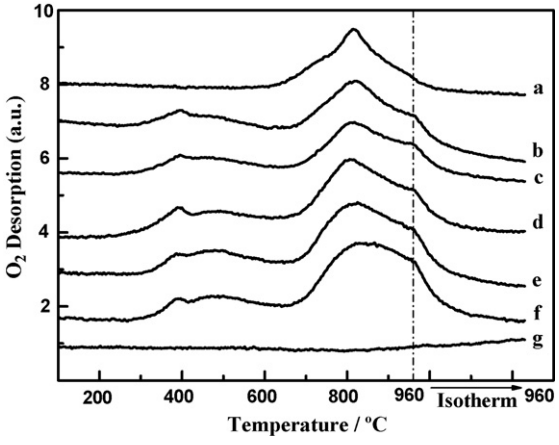

Fig. 1. O_2-TPD profiles of (a) LSM, (b) LSM–YSZ, (c) 1 wt% LDC–LSM–YSZ, (d) 3 wt% LDC–LSM–YSZ, (e) 5 wt% LDC–LSM–YSZ, (f) 10 wt% LDC–LSM–YSZ and (g) LDC.

3.2. Microstructures of the composite cathodes

Fig. 2 presents the SEM images and the corresponding EDX elemental images of the cell with the LSM–YSZ composite cath-

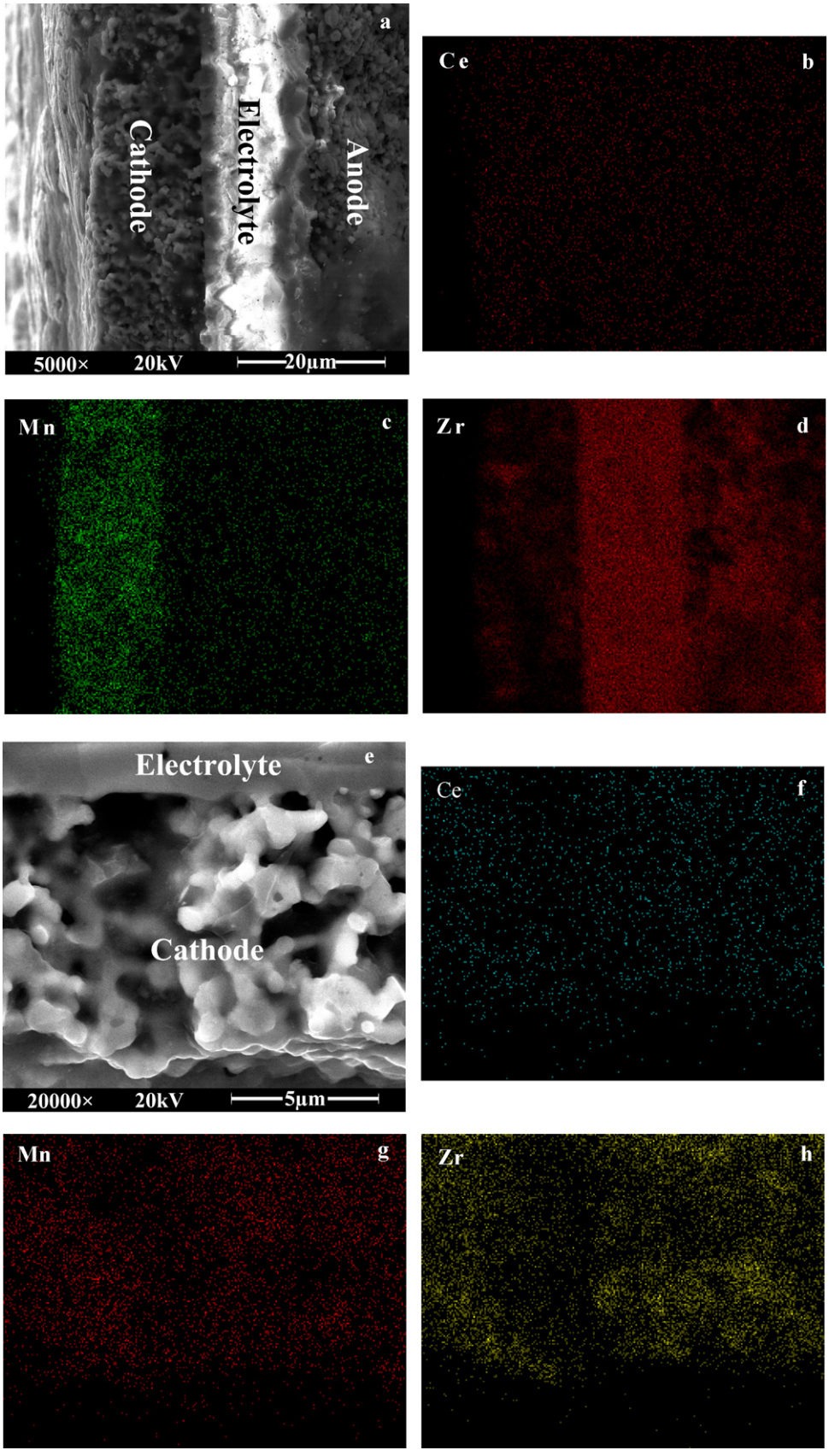

Fig. 2. SEM images and the corresponding EDX elemental images (f–h only include the cathode area in the cell) of cross-section of the cell with (a–d) LSM–YSZ composite cathode and (e–h) 10 wt% LDC–LSM–YSZ composite cathode. (a and e) SEM images, (b and f) SEM-EDX images of Ce, (c and g) SEM-EDX images of Mn, (d and h) SEM-EDX images of Zr.

ode and the 10 wt% LDC–LSM–YSZ composite cathode. For the cell with the LSM–YSZ composite cathode, the Mn element is distributed in the cathode, and the Zr element is distributed in cathode, electrolyte and anode. The EDX image of Ce element is obtained as a noise background. In the 10 wt% LDC–LSM–YSZ composite cathode, Ce, Mn and Zr elements are distributed in the total cathode. The distribution of Ce element is quite uniform.

Fig. 3 shows the SEM images and the EDX spectra of the surfaces of the LSM–YSZ composite cathode and the 10 wt% LDC–LSM–YSZ composite cathode. Obviously, there are two kinds of different morphologies in the LSM–YSZ composite cathode (Fig. 3a). EDX analysis depicts that the regular-shaped particles are LSM (Fig. 3b) and the fused-together ones without clear grain boundaries are YSZ (Fig. 3c). The size of LSM particles are in the range of 0.6–1 μm. Similarly, the regular-shaped LSM particles and fused YSZ particles can also be observed clearly on the 10 wt% LDC–LSM–YSZ composite cathode (Fig. 3d). Some fine particles with uniform size of 20–40 nm are observed on the surface of LSM particles in LDC–LSM–YSZ cathode, while no visible particles are observed on the surface of YSZ. EDX analysis shows these fine particles are LDC (Fig. 3e).

3.3. Cell performances

Fig. 4 presents the *I–V* curves and the corresponding power densities of single cells with different composite cathodes measured at different temperatures. The cell performance increases with the increase of LDC content in low LDC content range, reaches the maximum value at 10 wt% or 15 wt% LDC content, and then decreases with the further increase of LDC content. The above trend is more apparent when the operation temperature decreases. At 650 °C, the cells with

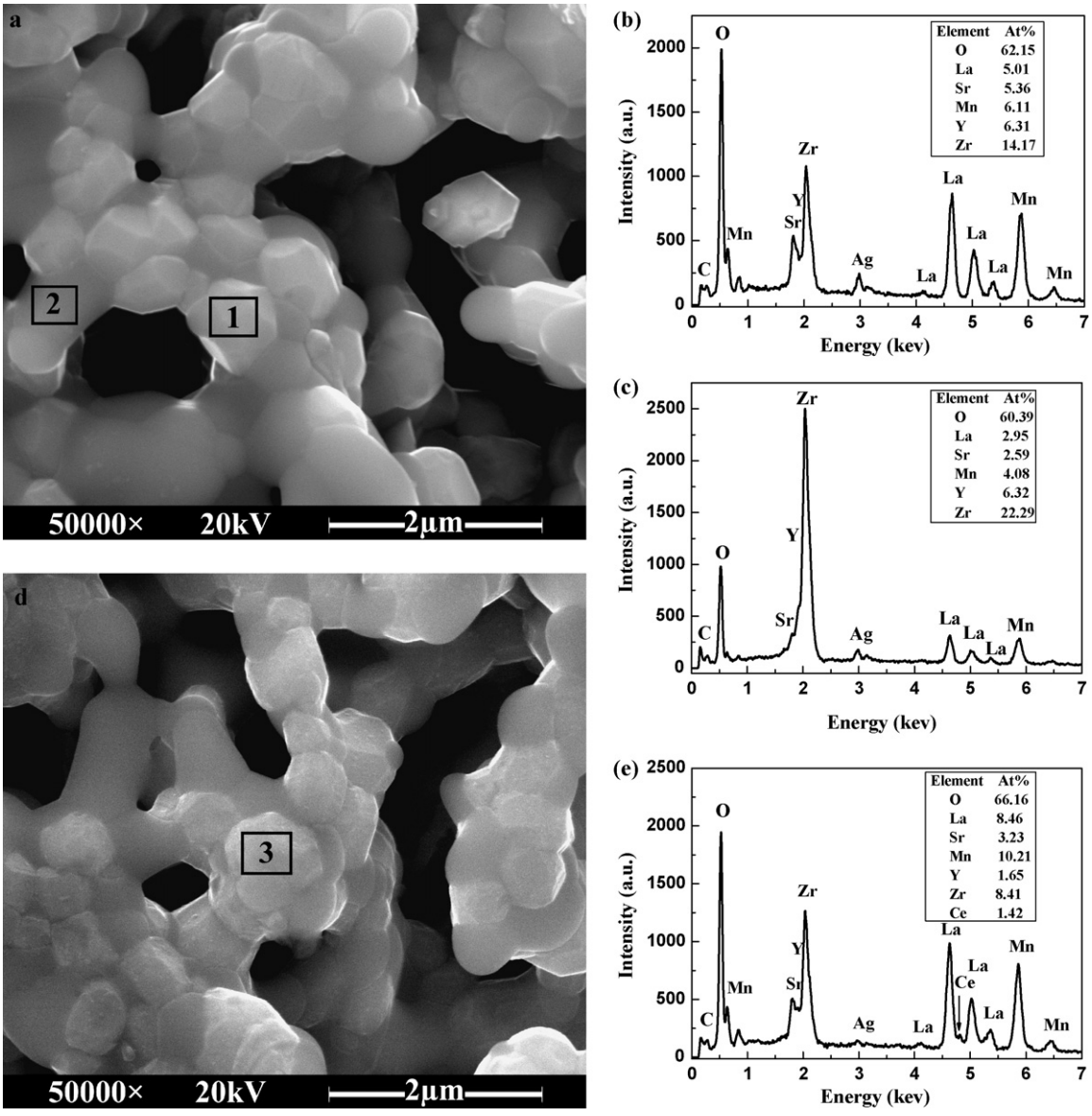

Fig. 3. SEM images and the EDX spectra of the surfaces of composite cathodes of (a–c) LSM–YSZ, (d and e) 10 wt% LDC–LSM–YSZ. (a and d) SEM images and (b, c and e) EDX spectra of areas 1, 2 and 3 marked by blank rectangle, respectively.

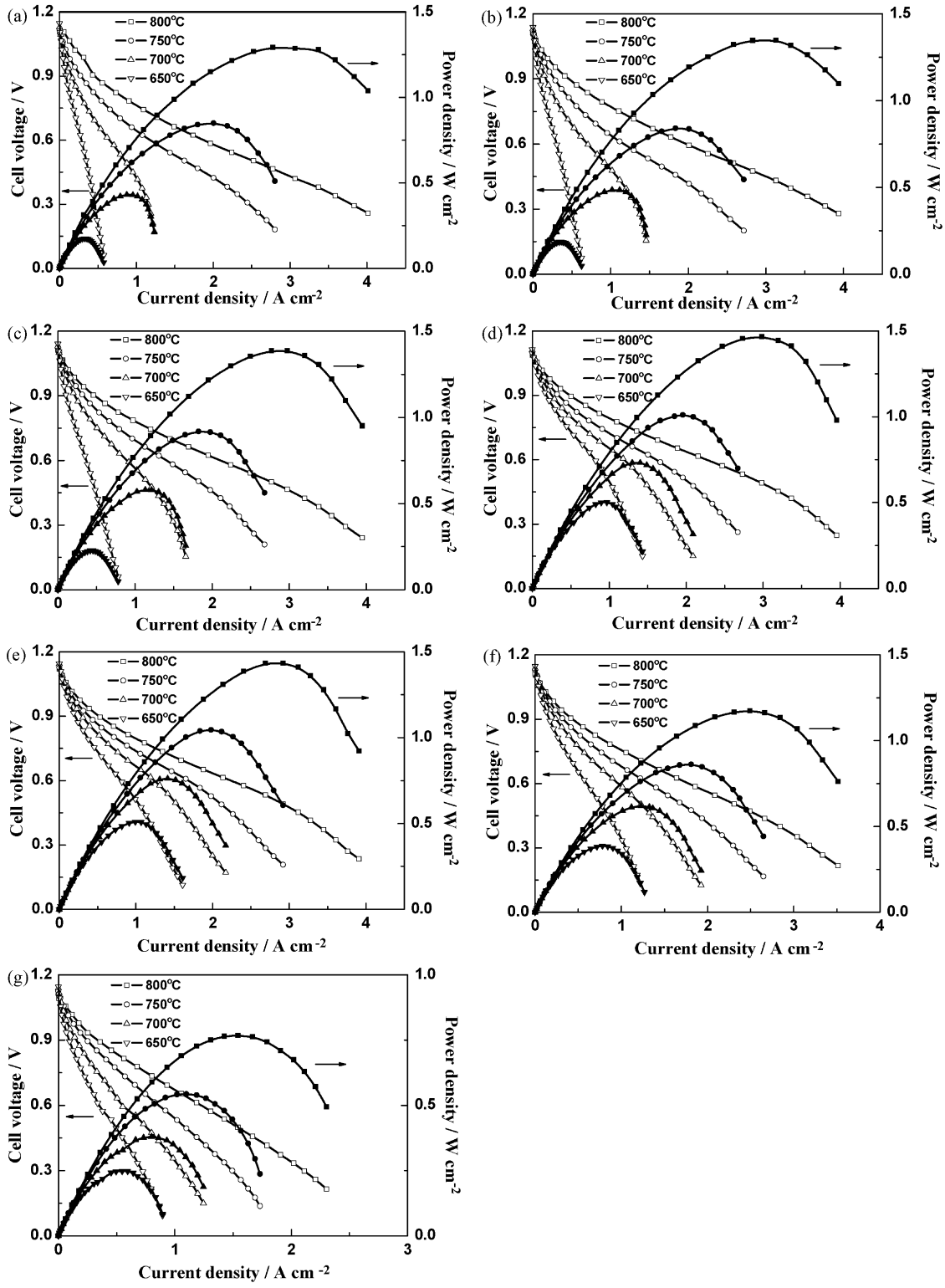

Fig. 4. *I–V* curves and the corresponding power densities of single cells with composite cathodes of (a) LSM–YSZ, (b) 1 wt% LDC–LSM–YSZ, (c) 5 wt% LDC–LSM–YSZ, (d) 10 wt% LDC–LSM–YSZ, (e) 15 wt% LDC–LSM–YSZ, (f) 20 wt% LDC–LSM–YSZ and (g) 50 wt% LDC–LSM–YSZ.

LSM–YSZ, 5 wt% LDC–LSM–YSZ, 10 wt% LDC–LSM–YSZ, 20 wt% LDC–LSM–YSZ, and 50 wt% LDC–LSM–YSZ composite cathodes give the maximum power densities (MPD) of 0.18 W cm^{-2}, 0.23 W cm^{-2}, 0.5 W cm^{-2}, 0.39 W cm^{-2} and 0.25 W cm^{-2}, respectively. The MPD, which is presented on the cell with the 10 wt% LDC–LSM–YSZ composite cathodes, is 2.8 times as high as that of the cell with the LSM–YSZ composite cathode. The cell with the 20 wt% LDC–LSM–YSZ composite cathode exhibits a lower MPD than the cell with the LSM–YSZ composite cathode at 800 °C, but it shows a higher MPD than

the cell with the LSM–YSZ composite cathode at a temperature below 800 °C. Compared with the cell with the LSM–YSZ composite cathode, the cell with the 50 wt% LDC–LSM–YSZ composite cathode shows a relative better performance at lower temperatures than at higher temperatures, and it is even better than that of the cell with the LSM–YSZ composite cathode at 650 °C. The above results indicate that the addition of LDC in the composite cathode improves the cell performance at lower operating temperatures.

3.4. Impedance analysis

EIS is a very sensitive and useful method for electrode activity investigation, which can provide information about the R_{ohm} as well as the R_p from the rate determining steps in the overall electrochemical processes. Fig. 5 shows Nyquist plots of single cells with different composite cathodes. Since the polarization of H_2 oxidation on a Ni-YSZ anode is much smaller than that of O_2 reduction on a LSM–YSZ composite cathode [29,30], the impedance spectra mainly reflect the properties of the cathodes. In order to eliminate the differences in anode and electrolyte in different cells, all the assemblies of anode/electrolyte were obtained from the same batch under the same fabrication conditions. The Nyquist plots show two arcs except for the cell with 50 wt% LDC–LSM–YSZ composite cathode. The smaller one located in high frequency range with the summit frequency of ca. 6309 Hz is related to the transport of oxygen anions across LSM/YSZ interfaces in addition to the transport through YSZ in the composite cathode [31]. Another one locating in low frequency range with the summit frequency ranging from ca. 125 Hz to ca. 15.8 Hz is the dominant contributor to the impedance, which is attributed to the dissociative adsorption of oxygen and diffusion of oxygen intermediates and/or oxygen anions on LSM surfaces and transfer of these species at TPBs [31]. At lower temperatures (≤700 °C), the high-frequency ends of the arcs intercept the real axis with 45° inclination angles. At higher temperatures (≥750 °C), the shapes of the arcs have a tendency towards semi-circle. As is shown in the magnified Nyquist plots in Fig. 5d, the high-frequency arc changes very little when LDC content is below 10 wt%, and it is suppressed when LDC content is above 10 wt%. Compared with the high-frequency arc, the low-frequency arc changes more obviously with LDC content. When LDC content is below 10 wt%, the low-frequency arc is gradually suppressed with the increase of LDC content, and when LDC content is over 15 wt%, the low-frequency arc is gradually enlarged. This tendency becomes more evident at lower temperatures.

In Nyquist plot, the highest frequency intercept on real axis represents the overall R_{ohm} from the electrolyte, the electrodes, the interfaces of cathode/electrolyte and anode/electrolyte and the connection wires. The lowest frequency intercept on real axis represents the overall resistance of the cell at open circuit voltage conditions. The distance between the two intercepts corresponds to R_p. Fig. 6 shows the change of MPD, R_{ohm} and

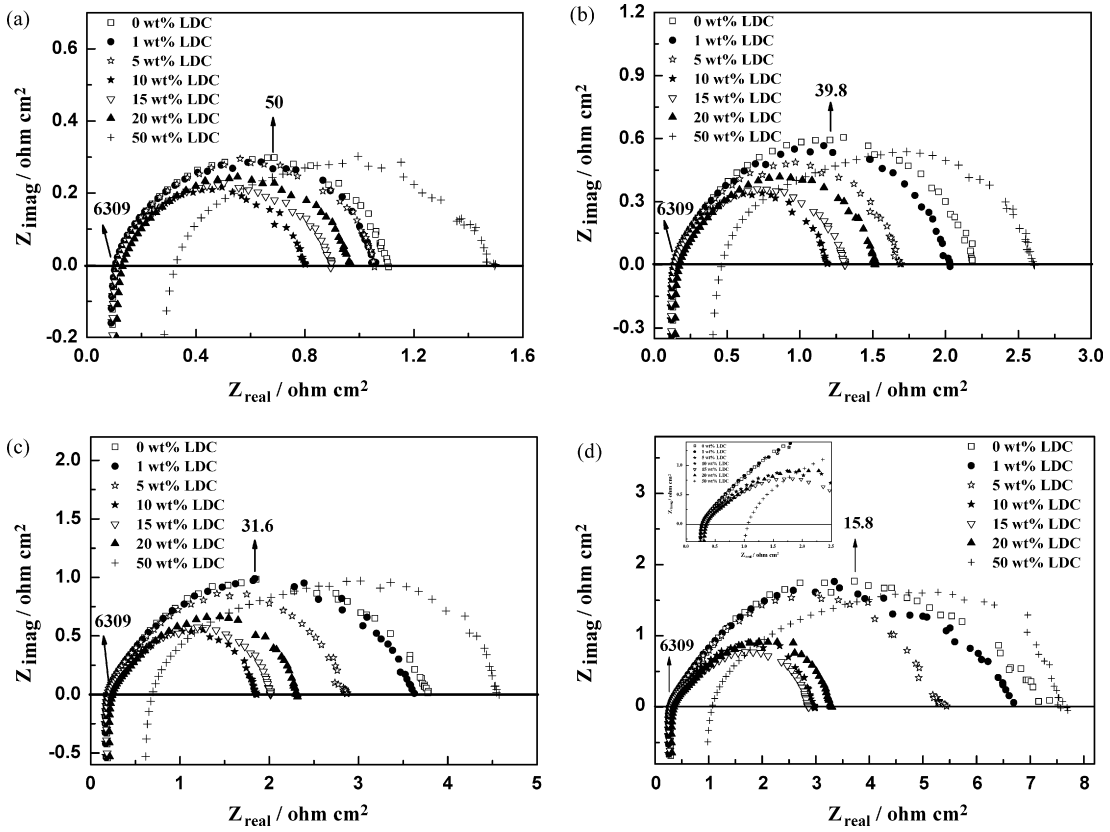

Fig. 5. Nyquist plots of single cells with different composite cathodes obtained at temperatures of (a) 800 °C, (b) 750 °C, (c) 700 °C and (d) 650 °C. The inset in (d) is the magnified Nyquist plots in high frequency range. The numbers in Figures are summit frequencies in Hz.

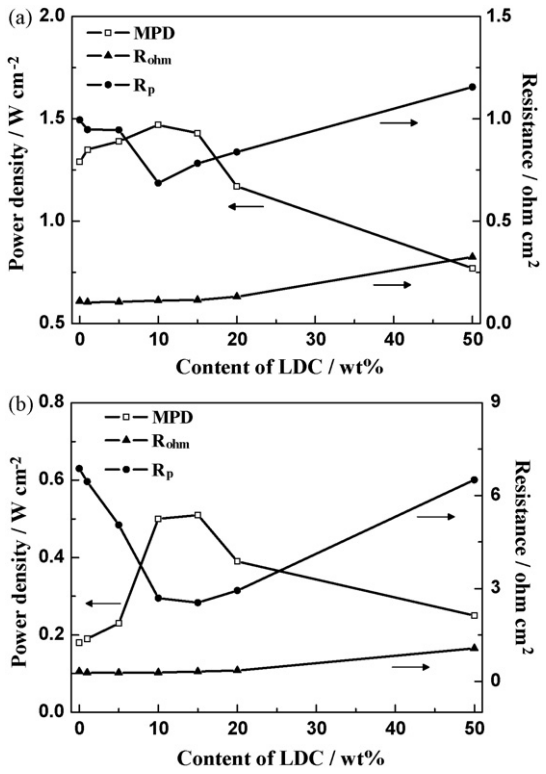

Fig. 6. Maximum power densities (MPD), ohmic resistances (R_{ohm}) and polarization resistances (R_p) of single cells with different composite cathodes measured at temperatures of (a) 800 °C and (b) 650 °C.

R_p of single cells with different LDC content in the composite cathodes. When the content of LDC is less than (or equal to) 10 wt%, R_{ohm} is almost unchanged, and it increases gradually when the content exceeds 10 wt%. For the cell with the 50 wt% LDC–LSM–YSZ composite cathode, R_{ohm} are 3 and 3.4 times of those of the cell with LSM–YSZ composite cathode at 800 °C and 650 °C, respectively. The increase of R_{ohm} is caused by the following two factors. The first one is the mismatch of thermal expansion coefficients between the high LDC content composite and the YSZ electrolyte film. During experiments, it was observed that the 50 wt% LDC–LSM–YSZ composite cathode easily detached from the surface of electrolyte film. The second one is the interruption of LSM network for electrical conduction due to the greatly reduced LSM content in the composite cathode with higher LDC content.

With the increase of LDC content, R_p decreases first, attains the minimum at 10 wt% or 15 wt% LDC and then increases. For the cell with the 10 wt% LDC–LSM–YSZ composite cathode, the R_p are 70% and 40% of those of the cell with LSM–YSZ composite cathode at 800 °C and 650 °C, respectively. Though at 800 °C the R_p of the cell with the 50 wt% LDC–LSM–YSZ composite cathode is higher than that of the cell with LSM–YSZ composite cathode, it is also lower than that of the cell with the LSM–YSZ composite cathode at 650 °C. The above results also depict that the addition of LDC in composite cathode is of benefit for the cell operating at lower temperatures.

As the frequency data cannot be observed directly in Nyquist plots, the Bode plots of some single cells are given in Fig. 7. In a Bode plot, peaks in the imaginary parts correspond to the

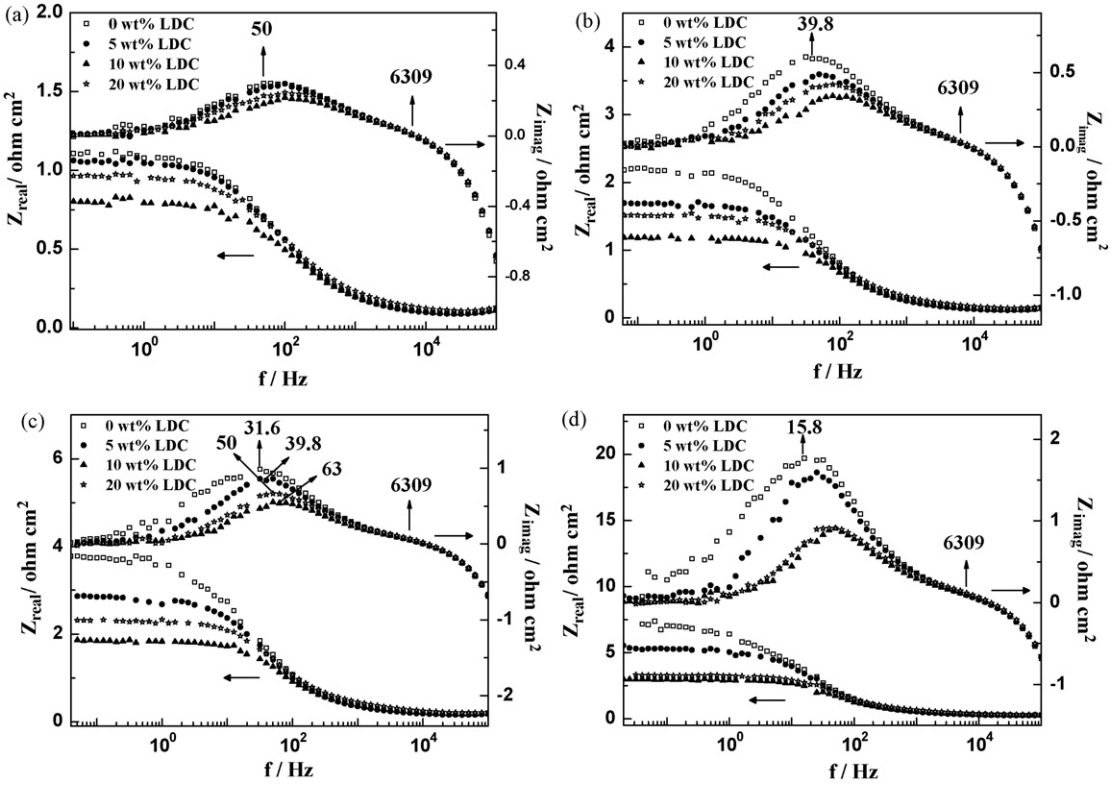

Fig. 7. Bode plots of single cells with different composite cathodes obtained at temperatures of (a) 800 °C, (b) 750 °C, (c) 700 °C and (d) 650 °C. The numbers in Figures are summit frequencies in Hz.

summit frequencies of physicochemical processes. It can be observed that the summit frequencies of the high-frequency arcs remain approximately unchanged with the increase of LDC content, whereas the summit frequencies of the low-frequency arcs increase first when the LDC content is below 10 wt%, and then decrease a little. The summit frequencies of the low-frequency arcs of the cells with the LSM–YSZ, 5 wt% LDC–LSM–YSZ, 10 wt% LDC–LSM–YSZ and 20 wt% LDC–LSM–YSZ composite cathodes at 700 °C are 31.6 Hz, 39.8 Hz, 63 Hz and 50 Hz, respectively, suggesting the acceleration of the related electrochemical process. This change tendency is opposite to that of the resistance related to the low-frequency arc because the summit frequency is equal to $1/RC$. The summit frequency of the low-frequency arc is also affected by the operation temperature. With the operation temperature increasing, the summit frequency of the low-frequency arc increases. For the cell with the LSM–YSZ composite cathode, it changes from ca. 15.8 Hz, 31.6 Hz, 39.8 Hz to ca. 50 Hz from 650 °C, 700 °C, 750 °C to 800 °C. These changes reflect that the process related to the low-frequency arc is accelerated when the temperature is elevated.

When LDC content is below 10 wt% or 15 wt%, both Nyquist plots and Bode plots indicate that the physicochemical process reflected by the low-frequency arc, i.e. the dissociative adsorption of oxygen and diffusion of oxygen intermediates and/or oxygen ions on LSM surface and transfer of species at TPBs, is accelerated with the increase of LDC content. This phenomenon results from the formation of more oxygen vacancies as we mentioned in Section 3.1. The special redox property of Ce^{4+} and Ce^{3+} makes it easy to release an electron for Ce^{3+} to become Ce^{4+}, concomitantly with the formation of oxygen vacancies on LSM surfaces, which can be expressed as the Eqs. (3) and (4)

$$O^{x}_{O,LSM} + 2Mn^{\bullet}_{Mn,LSM} + V^{\bullet\bullet}_{O,LDC} + 2e' \rightarrow V^{\bullet\bullet}_{O,LSM} + 2Mn^{x}_{Mn,LSM} + O^{x}_{O,LDC} \quad (3)$$

$$O^{x}_{O,LSM} + 2Mn^{x}_{Mn,LSM} + V^{\bullet\bullet}_{O,LDC} + 2e' \rightarrow V^{\bullet\bullet}_{O,LSM} + 2Mn'_{Mn,LSM} + O^{x}_{O,LDC} \quad (4)$$

where $O^{x}_{O,LDC}$ represents the O^{2-} ions in LDC lattice sites; $V^{\bullet\bullet}_{O,LDC}$stands for oxygen vacancies. The fine LDC particles on LSM particles, as observed in SEM image, provide more reaction sites. The role of oxygen vacancies has been confirmed by many researchers. Winter [32] pointed out that some surface trap states of oxygen vacancies in oxides could be active sites for the adsorption and the dissociation of oxygen. De Souza and Kilner [33] observed that oxygen vacancies in $La_{1-x}Sr_xMn_{1-y}Co_yO_{3\pm\delta}$ affected remarkably oxygen surface exchange rate and oxygen diffusion coefficient. The above facts verify that oxygen vacancies play a major role in the oxygen surface exchange process for acceptor-doped perovskites like LSM. The more oxygen vacancies created on LSM surfaces may increase active sites for oxygen reduction, thus facilitate the oxygen reduction processes.

When LDC content is above 10 wt% or 15 wt%, the electrochemical process reflected by the low-frequency arc becomes slightly slower with the increase of LDC content. This phenomenon arises from the decrease of TPBs due to the decreased LSM content. For the 50 wt% LDC–LSM–YSZ composite cathode, the excessive LDC and the extreme low LSM content lead to the significant reduction of TPBs. Thus, the oxygen reduction process in the cell with 50 wt% LDC–LSM–YSZ composite cathode is quite different from the others.

4. Conclusions

LDC–LSM–YSZ composites with different LDC contents were fabricated to use as cathode materials of anode-supported IT-SOFCs. The O_2-TPD results depict that the addition of LDC promotes oxygen desorption, which may result from an increase of surface oxygen vacancies. The electrochemical results also show that the addition of LDC drastically suppressed the low frequency impedance arc, which indicates that the introducing of LDC facilitates the dissociative adsorption of oxygen and diffusion of oxygen intermediates and/or oxygen ions on LSM surface and transfer of species at TPBs. The optimized LDC content is about 10–15 wt% in the composite cathode. The MPD of the cell with 10 wt% LDC–LSM–YSZ composite cathode is 2.8 times of that of the cell with the LSM–YSZ composite cathode at 650 °C. The LDC–LSM–YSZ composite is a better cathode material for IT-SOFCs than the LSM–YSZ composite, especially at lower operation temperatures.

Acknowledgements

The authors gratefully acknowledge financial supports from the Ministry of Science and Technology of China (No. 2004CB719506, 2005CB221404 and 2006AA05Z147) and National Natural Science Foundation of China (No. 20676132).

References

[1] B.C.H. Steele, A. Heinzel, Nature 414 (2001) 345–352.
[2] S. de Souza, S.J. Visco, L.C. De Jonghe, Solid State Ionics 98 (1997) 57–61.
[3] H. Yokokawa, N. Sakai, T. Horita, K. Yamaji, Fuel Cells 1 (2001) 117–131.
[4] M.J.L. Ostergard, C. Clausen, C. Bagger, M. Mogensen, Electrochem. Acta 40 (1995) 1971–1981.
[5] B.C.H. Steele, Solid State Ionics 134 (2000) 3–20.
[6] O. Yamamoto, Electrochim. Acta 45 (2000) 2423–2435.
[7] T. Kenjo, M. Nishiya, Solid State Ionics 57 (1992) 295–302.
[8] T. Tsai, S.A. Barnett, Solid State Ionics 93 (1997) 207–217.
[9] Z. Bi, M. Cheng, Y. Dong, H. Wu, Y. She, B. Yi, Solid State Ionics 176 (2005) 655–661.
[10] V. Dusastre, J.A. Kilner, Solid State Ionics 126 (1999) 163–174.
[11] Z. Shao, S.M. Haile, Nature 431 (2004) 170–174.
[12] Z. Duan, M. Yang, A. Yan, Z. Hou, Y. Dong, Y. Chong, M. Cheng, W. Yang, J. Power Sources 160 (2006) 57–64.
[13] T. Hibino, A. Hashimoto, T. Inoue, J. Tokuno, S. Yoshida, M. Sano, Science 288 (2000) 2031–2033.
[14] S.P. Simner, J.P. Shelton, M.D. Anderson, J.W. Stevenson, Solid State Ionics 161 (2003) 11–18.
[15] G.C. Kostogloudis, G. Tsiniarakis, C. Ftikos, Solid State Ionics 135 (2000) 529–535.
[16] T. Tsai, S.A. Barnett, Solid State Ionics 98 (1997) 191–196.
[17] M. Shiono, K. Kobayashi, T.L. Nguyen, K. Hosoda, T. Kato, K. Ota, M. Dokiya, Solid State Ionics 170 (2004) 1–7.

[18] T. Horita, N. Sakai, H. Yokogawa, M. Dokiya, T. Kawada, J. Van Herle, K. Sasaki, J. Electroceram. 1 (1977) 155–164.
[19] R. Chiba, F. Yoshimura, Y. Sakurai, Y. Tabata, M. Arakawa, Solid State Ionics 175 (2004) 23–27.
[20] K. Yamahara, C.P. Jacobson, S.J. Visco, X.F. Zhang, L.C. De Jonghe, Solid State Ionics 176 (2005) 275–279.
[21] Z. Wang, M. Cheng, Y. Dong, M. Zhang, H. Zhang, Solid State Ionics 176 (2005) 2555–2561.
[22] S. Royer, A. Van Neste, R. Davidson, S. McIntyre, S. Kaliaguine, Ind. Eng. Chem. Res. 43 (2004) 5670–5680.
[23] C.H. Wang, C.L. Chen, H.S. Weng, Chemosphere 57 (2004) 1131–1138.
[24] S. Royer, F. Berube, S. Kaliaguine, Appl. Catal. A: Gen. 282 (2005) 273–284.
[25] J.H. Kuo, H.U. Anderson, D.M. Sparlin, J. Solid State Chem. 83 (1989) 52–60.
[26] J. Mizusaki, N. Mori, H. Takai, Y. Yonemura, H. Minamiue, H. Tagawa, M. Dokiya, H. Inaba, K. Naraya, T. Sasamoto, T. Hashimoto, Solid State Ionics 129 (2000) 163–177.
[27] M.-F. Luo, Z.-Y. Pu, M. He, J. Jin, L.-Y. Jin, J. Mol. Catal. A: Chem. 260 (2006) 152–156.
[28] Y.N. Lee, R.M. Lago, J.L.G. Fierro, J. González, Appl. Catal. A: Gen. 215 (2001) 245–256.
[29] S. de Souza, S.J. Visco, L.C. De Jonghe, J. Electrochem. Soc. 144 (1997) L35–L37.
[30] Y. Jiang, A.V. Virkar, F. Zhao, J. Electrochem. Soc. 148 (2001) A1091–A1099.
[31] M.J. Jørgensen, M. Mogensen, J. Electrochem. Soc. 148 (2001) A433–A442.
[32] E.R.S. Winter, J. Chem. Soc. A (1968) 2889–2902.
[33] R.A. De Souza, J.A. Kilner, Solid State Ionics 126 (1999) 153–161.